



² Supporting Information for

³ Forecasting range shifts of a dioecious plant species under climate change

⁴ Jacob K. Moutouama, Aldo Compagnoni and Tom E.X. Miller

⁵ Jacob Moutouama.

⁶ E-mail: jmoutouama@gmail.com

⁷ This PDF file includes:

⁸ Supporting text

⁹ Figs. S1 to S25

¹⁰ SI References

11 **Supporting Information Text**

12 **Supporting Methods**

13 **A. Climatic data collection.** The general circulation models (GCMs) were selected from the Coupled Model Intercomparison
14 Project Phase 5 (CMIP5): Model for Interdisciplinary Research on Climate (MIROC5), Australian Community Climate and
15 Earth System Simulator (ACCESS1-3), Community Earth System Model (CESM1-BGC), Centro Euro-Mediterraneo sui
16 Cambiamenti Climatici Climate Model (CMCC-CM). All the GCMs were also downloaded from Chelsa (1). We evaluated future
17 climate projections from two scenarios of representative concentration pathways (RCPs): RCP4.5, an intermediate-to-pessimistic
18 scenario assuming a radiative forcing amounting to 4.5 Wm^{-2} by 2100, and RCP8.5, a pessimistic emission scenario which
19 projects a radiative forcing of 8.5 Wm^{-2} by 2100 (2, 3).

20 Projection data for the three 30-year periods included warmer or colder conditions than observed in our experiment, so
21 extending our inferences to these conditions required some extrapolation. However, across all sites, both study years were
22 1–2°C warmer than their corresponding “current” (1990–2019) temperature normals (Fig. S25). Additionally, the 2014–15
23 growing season was generally wetter and cooler across the study region than 2015–16 (Fig. S25). Combined, the geographic
24 and inter-annual replication of the common garden experiment provided good coverage of most past and future conditions
25 throughout the study region (Fig. 1).

26 **B. Sex-specific demographic responses to climatic variation across common garden sites.** Vital rate models were fit with the
27 same linear predictors for the expected value (μ) (Eq. 1):

$$\begin{aligned}\mu = & \beta_0 + \beta_1 size + \beta_2 sex + \beta_3 pptgrow + \beta_4 pptdorm + \beta_5 tempgrow + \beta_6 tempdorm \\ & + \beta_7 pptgrow * sex + \beta_8 pptdorm * sex + \beta_9 tempgrow * sex + \beta_{10} tempdorm * sex \\ & + \beta_{11} size * sex + \beta_{12} pptgrow * tempgrow + \beta_{13} pptdorm * tempdorm \\ & + \beta_{14} pptgrow * tempgrow * sex + \beta_{15} pptdorm * tempdorm * sex + \beta_{16} pptgrow^2 \\ & + \beta_{17} pptdorm^2 + \beta_{18} tempgrow^2 + \beta_{19} tempdorm^2 + \beta_{20} pptgrow^2 * sex \\ & + \beta_{21} pptdorm^2 * sex + \beta_{22} tempgrow^2 * sex + \beta_{23} tempdorm^2 * sex + \phi + \rho + \nu\end{aligned}\quad [1]$$

29 where β_0 is the grand mean intercept, β_1 is the size dependent slopes. *size* was on a natural logarithm scale. $\beta_2 \dots \beta_{13}$ represent
30 the climate dependent slopes. $\beta_{14} \dots \beta_{23}$ represent the sex-climate interaction slopes. *pptgrow* is the precipitation of the growing
31 season, *tempgrow* is the temperature of the growing season, *pptdorm* is the precipitation of the dormant season, *tempdorm* is
32 the temperature of the dormant season.

33 All vital rates were fit with second-degree polynomial functions to accommodate the possibility of hump-shaped relationships
34 (reduced demographic performance at both extremes). We also included two-way interactions between sex and each climate
35 driver and between temperature and precipitation within each season, and a three-way interaction between sex, temperature,
36 and precipitation within each season. We modeled survival and flowering data with a Bernoulli distribution and the growth
37 (tiller number) with a zero-truncated Poisson inverse Gaussian distribution. Fertility (panicle count conditional on flowering)
38 was modeled as zero-truncated negative binomial. We used generic, weakly informative priors to fit coefficients for survival,
39 growth, flowering models ($\beta \sim N(0, 1.5)$) and random effect variances ($\sigma \sim \text{Gamma}(\gamma(0.1, 0.1))$). We fit fertility model with
40 also weakly informative priors for coefficients ($\beta \sim N(0, 0.15)$). Different priors were used for fertility because the panicle
41 model has a large number of parameters relative to the amount of available data (subset of our data) and because these
42 specifics priors help prevent the model from overfitting. Each vital rate also includes normally distributed random effects for
43 block-to-block variation ($\phi \sim N(0, \sigma_{block})$), site to site variation ($\nu \sim N(0, \sigma_{site})$), and source-to-source variation that is
44 related to the genetic provenance of the transplants used to establish the common garden ($\rho \sim N(0, \sigma_{source})$).

45 **C. Sex ratio responses to climatic variation across common garden sites.** To understand the impact of climatic variation across
46 common garden sites on sex ratio, OSR and SR models using the same linear predictors for the expected value (ν) (Eq. 2):

$$\begin{aligned}\nu = & \omega_0 + \omega_1 pptgrow + \omega_2 pptdorm + \omega_3 tempgrow + \omega_4 tempdorm + \\ & \omega_5 pptgrow^2 + \omega_6 pptdorm^2 + \omega_7 tempgrow^2 + \omega_8 tempdorm^2 + \epsilon\end{aligned}\quad [2]$$

48 where *OSR* is the proportion of panicles that were female or proportion of female individuals in the experimental populations,
49 *c* is the climate. ω_0 is the intercept, $\omega_1, \dots, \omega_8$ are the climate dependent slopes. ϵ is error term.

50 We modeled the OSR and SR data with a Bernoulli distribution and used non informative priors for each coefficient
51 ($\omega \sim N(0, 100)$).

52 **D. Sex ratio experiment.** To estimate the probability of seed viability, the germination rate and the effect of sex-ratio variation
53 on female reproductive success, we conducted a sex-ratio experiment at one site near the center of the range to estimate the
54 effect of sex-ratio variation on female reproductive success. The details of the experiment are provided in (4) and (5). Here
55 we provide a summary of the experiment. We established 124 experimental populations in plots measuring $0.4 \times 0.4\text{m}$ and
56 separated by at least 15m from each other. We varied population density (1–48 plants/plot) and sex ratio (0%–100% female)
57 across the experimental populations, and we replicated 34 combinations of density and sex ratio. We collected panicles from

58 a subset of females in each plot and recorded the number of seeds in each panicle. We assessed reproductive success (seeds
59 fertilized) using greenhouse-based germination and trazolium-based seed viability assays. Seed viability was modeled with a
60 binomial distribution where the probability of viability (v) was given by:

61
$$v = v_0 * (1 - OSR^\alpha) \quad [3]$$

62 where OSR is the proportion of panicles that were female in the experimental populations. α is the parameter that control for
63 how viability declines with increasing female bias. Further, germination rate was modeled using a binomial distribution to
64 model the germination data from greenhouse trials. Given that germination was conditional on seed viability, the probability
65 of success was given by the product $v * g$, where v is a function of OSR (Eq. 3) and g is assumed to be constant.

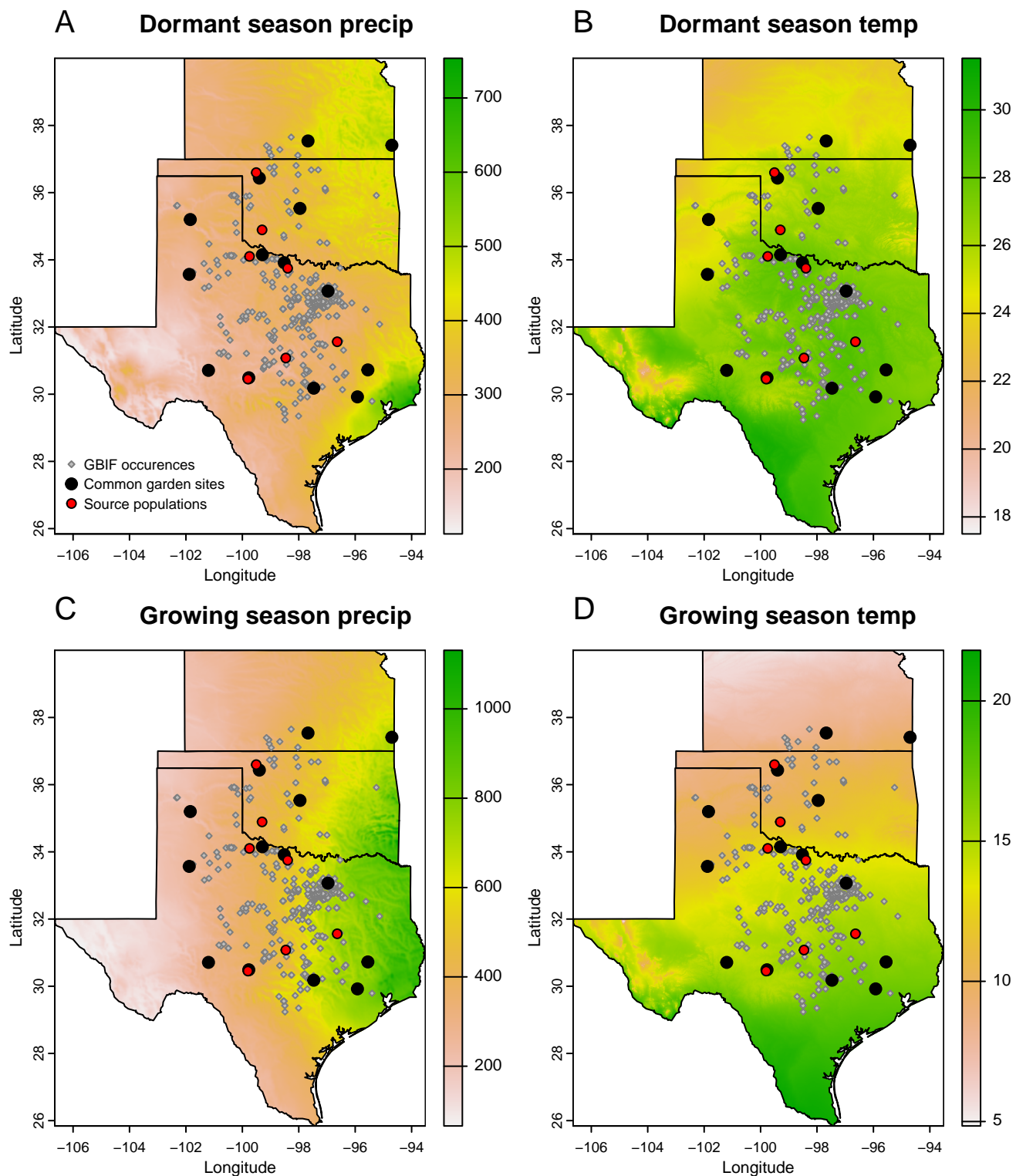


Fig. S1. texbfMaps of 30-year (1990–2019) climate normals and study sites used for demographic monitoring of *Poa arachnifera* in Texas, Kansas and Oklahoma in the United States. Precipitation is in mm and temperature is in °C. We surveyed 22 natural populations (grey diamond). The common garden sites were installed on 14 sites (black circle) collected from 7 source populations (red circle)

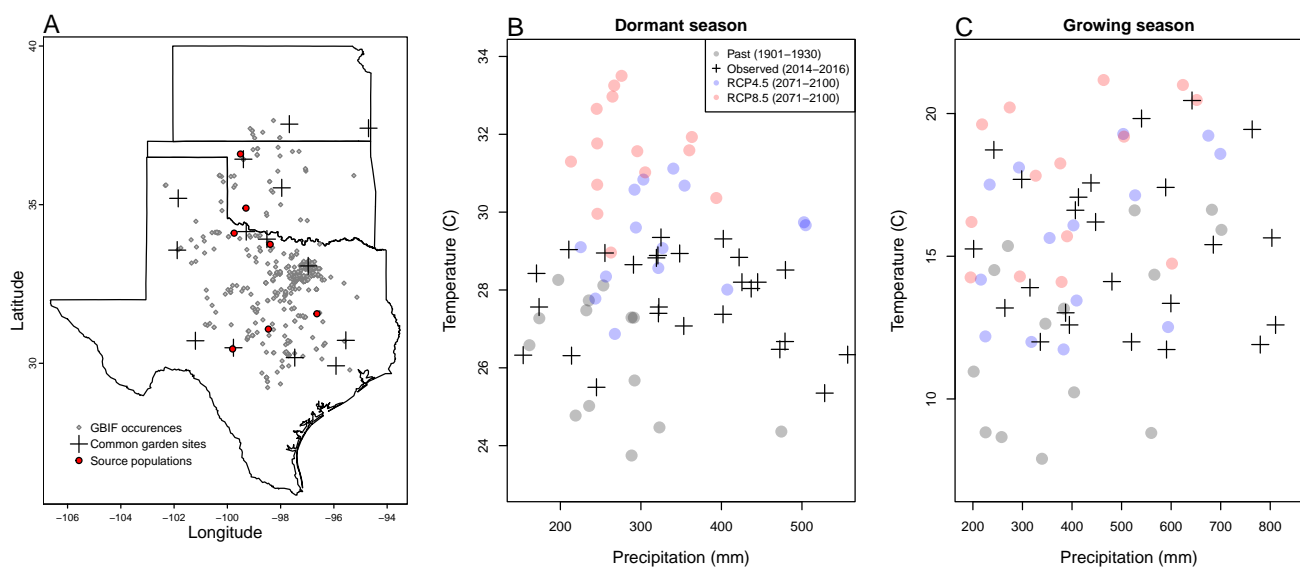


Fig. S2. Experimental gardens and climate of the study region. **A:** Map of 14 experimental garden sites (crosses) in Texas, Oklahoma, and Kansas relative to GBIF occurrences of *Poa arachnifera* (gray points). Red points indicate source populations for plants used in the common garden experiment. **B,C:** Past, future, and observed climate space for growing and dormant seasons. Crosses show observed conditions for the sites and years of the common garden experiment. Gray points show historical (1901–1930) climate normals, and blue and red points show end-of-century (2071–2100) climate normals for RCP4.5 and RCP8.5 projections, respectively, from MIROC5.

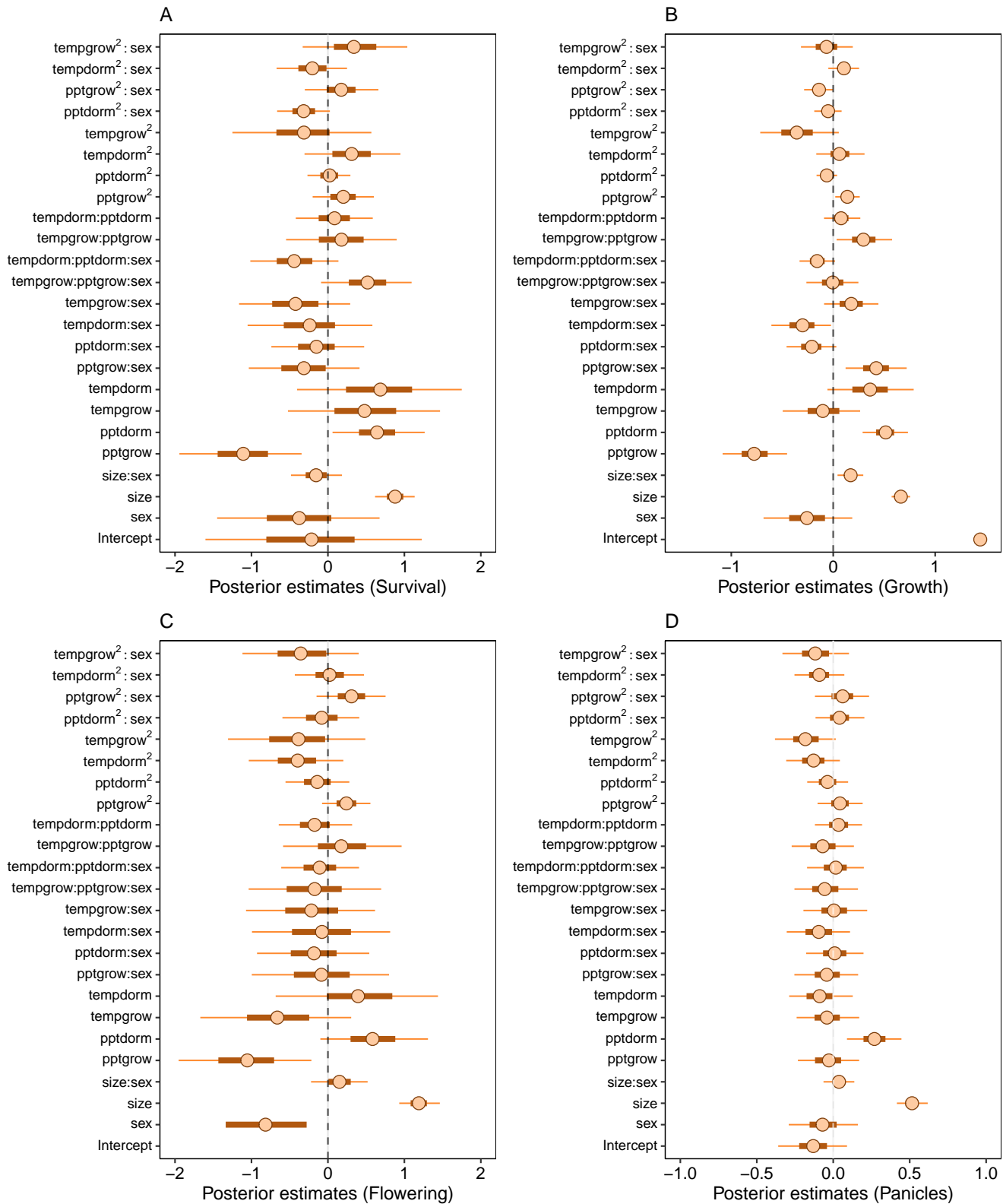


Fig. S3. Mean parameter values and 95% credible intervals of the posterior probability distributions. pptgrow is the precipitation of growing season, Tempgrow is the temperature of growing season, Tempdorm is the temperature of dormant season, Pptdorm is the precipitation of dormant season.

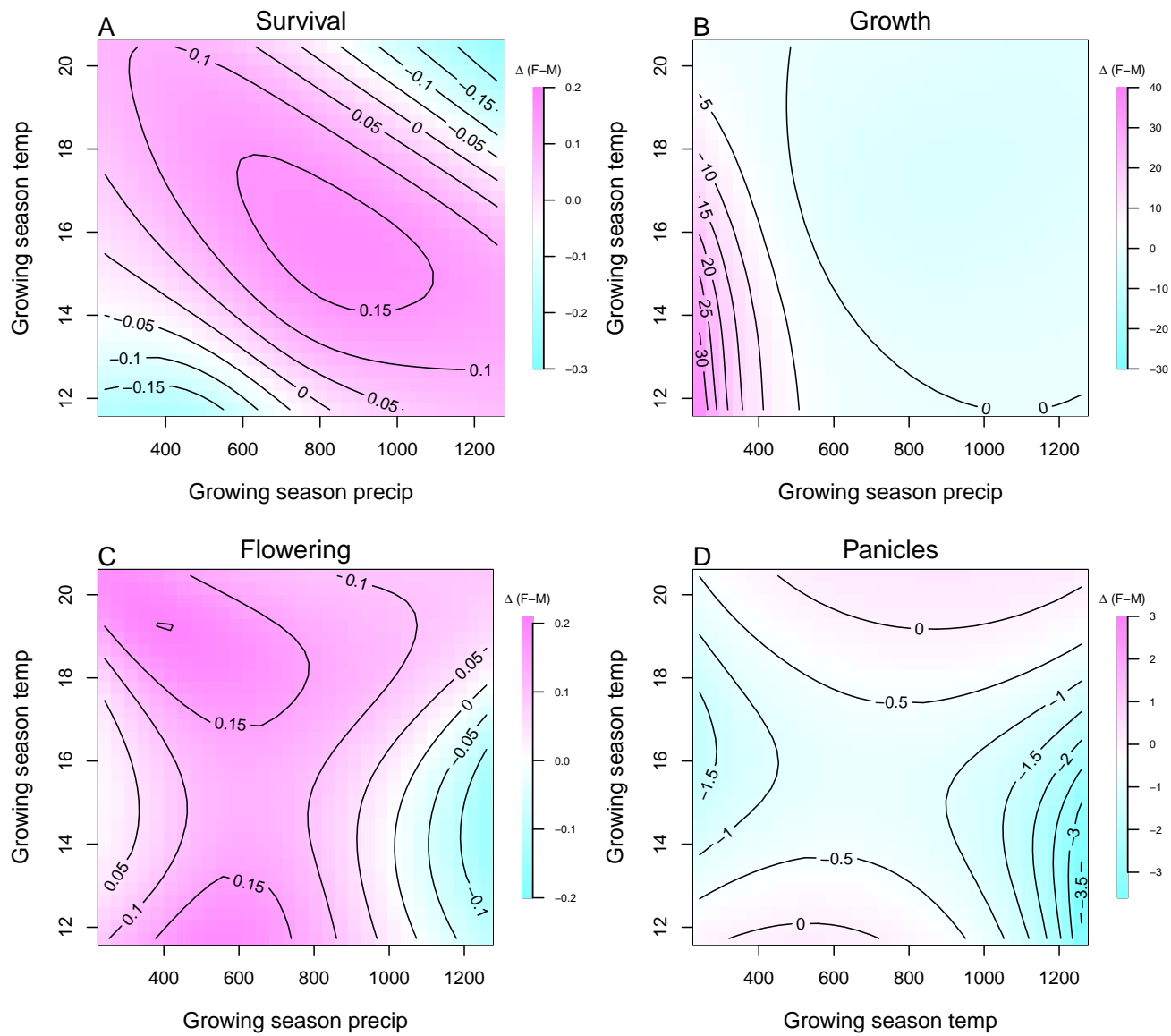


Fig. S4. Predicted difference in demographic response to climate across species range between female and male. Contours show predicted value of that difference conditional on precipitation and temperature of growing season

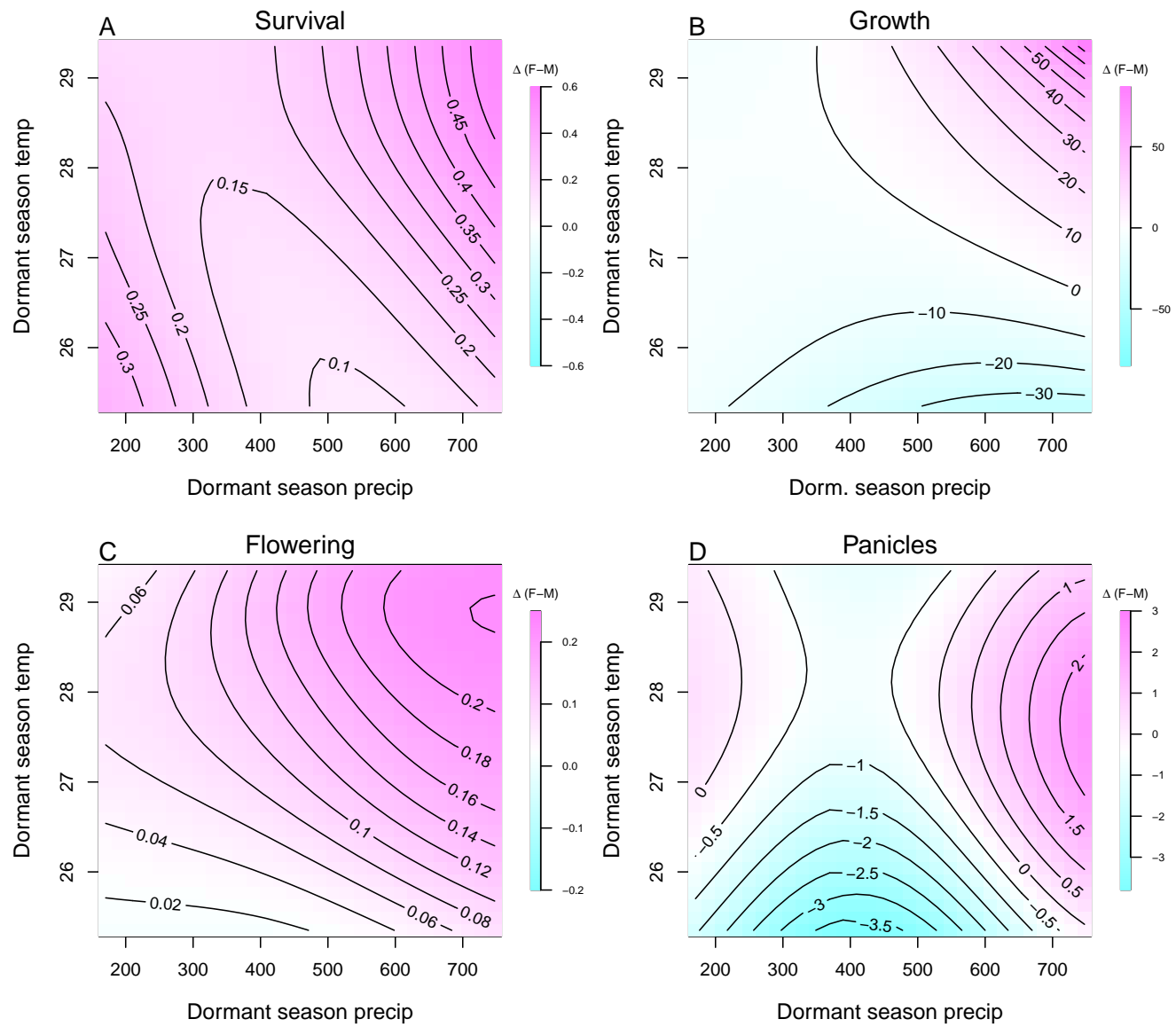


Fig. S5. Predicted difference in demographic response to climate across species range between female and male. Contours show predicted value of that difference conditional on precipitation and temperature of the dormant season

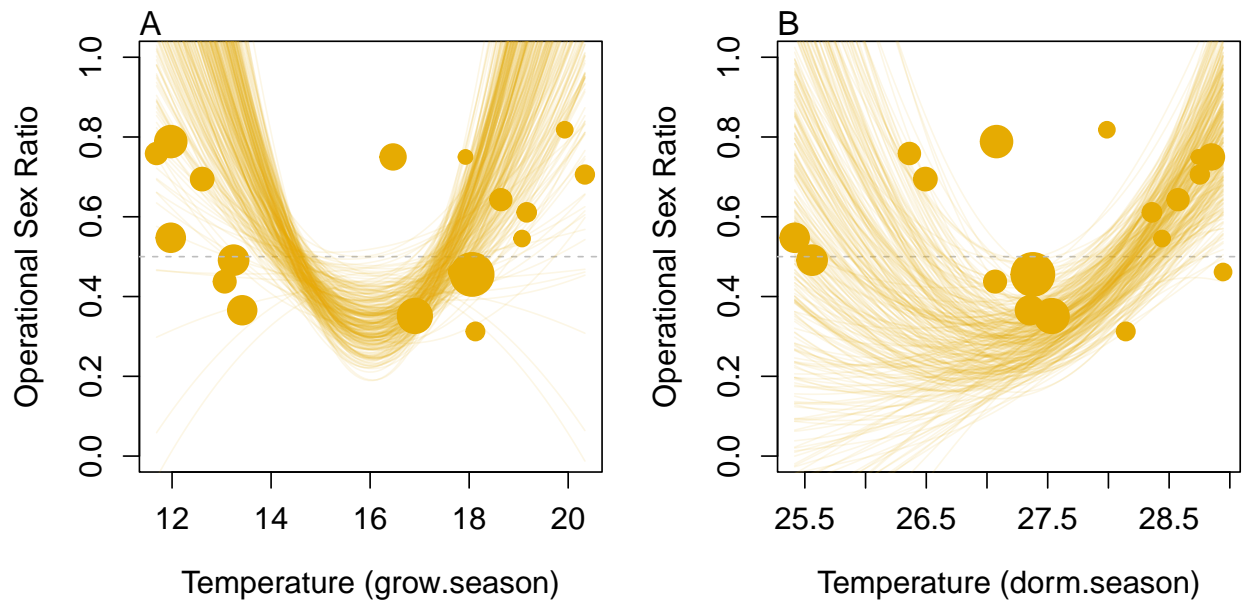


Fig. S6. Significant Operational Sex Ratio response across climate gradient. (A, B) Proportion of panicles that were females across temperature of the growing and dormant season. Each line represents a posterior sample. We used (300 posterior samples)

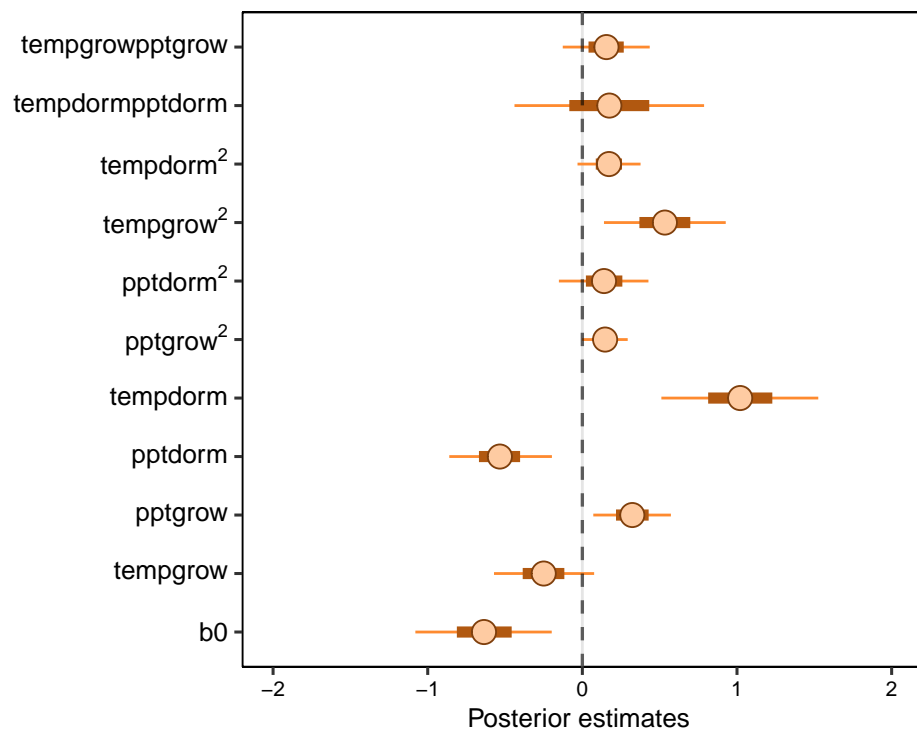


Fig. S7. Mean parameter values and 95% credible intervals of the posterior probability distributions for climate drivers of operational sex ratio (female fraction of total panicles) across common garden years and sites. pptgrow is the precipitation of growing season, Tempgrow is the temperature of growing season, pptdorm is the temperature of dormant season, Tempdorm is the temperature of dormancy season.

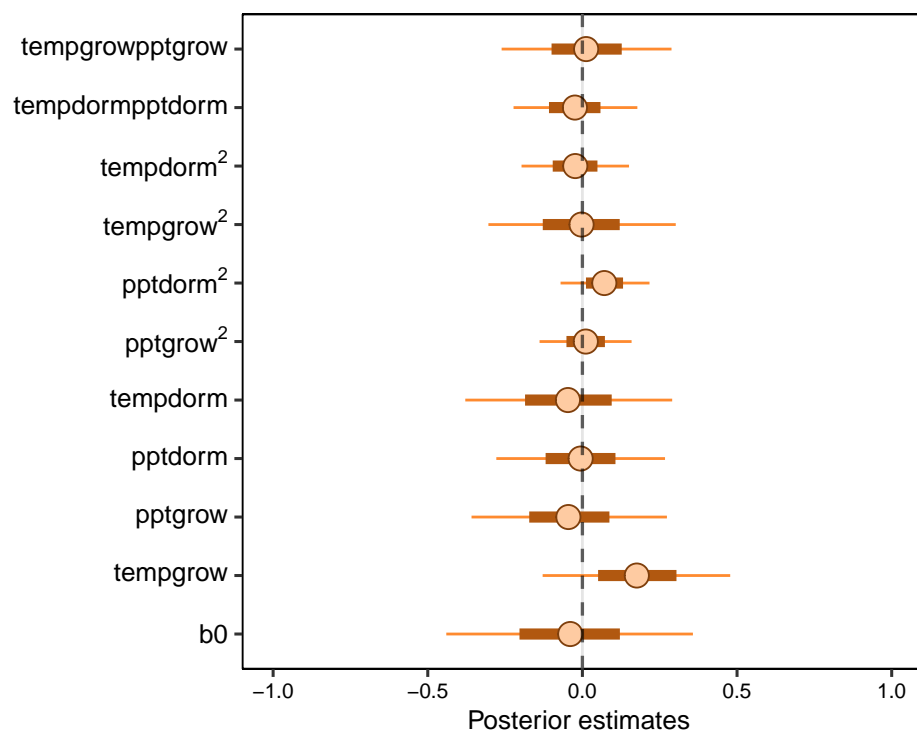


Fig. S8. Mean parameter values and 95% credible intervals of the posterior probability distributions for climate drivers of sex ratio (female fraction of the populations) across common garden years and sites. pptgrow is the precipitation of growing season, Tempgrow is the temperature of growing season, pptdorm is the temperature of dormant season, Tempdorm is the temperature of dormancy season.

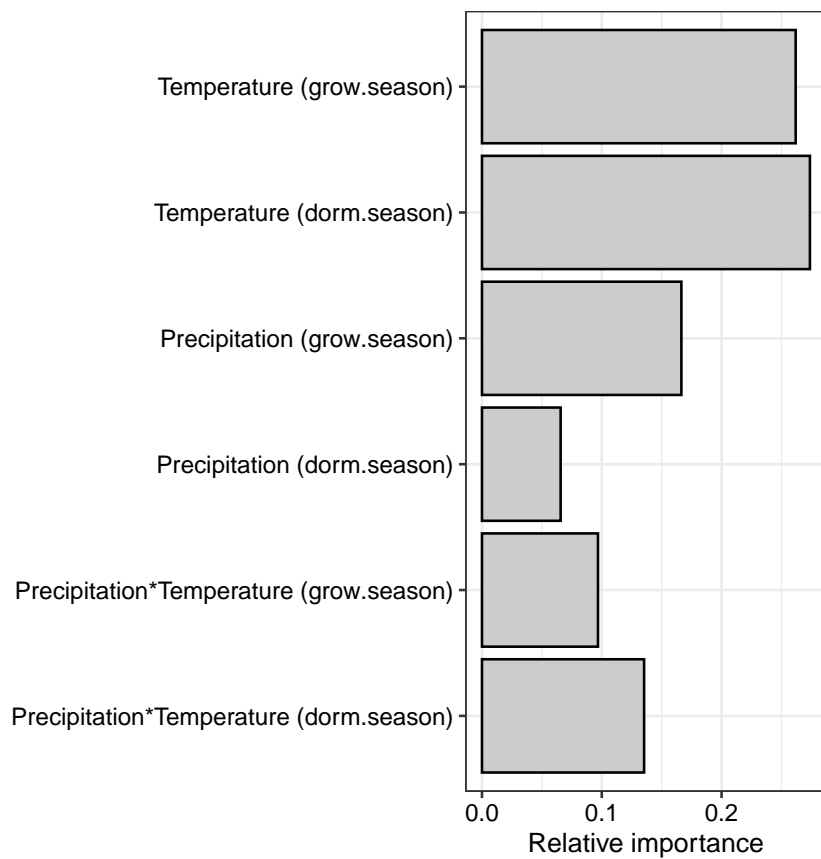


Fig. S9. Life Table Response Experiment: The bar represent the relative importance of each predictors.

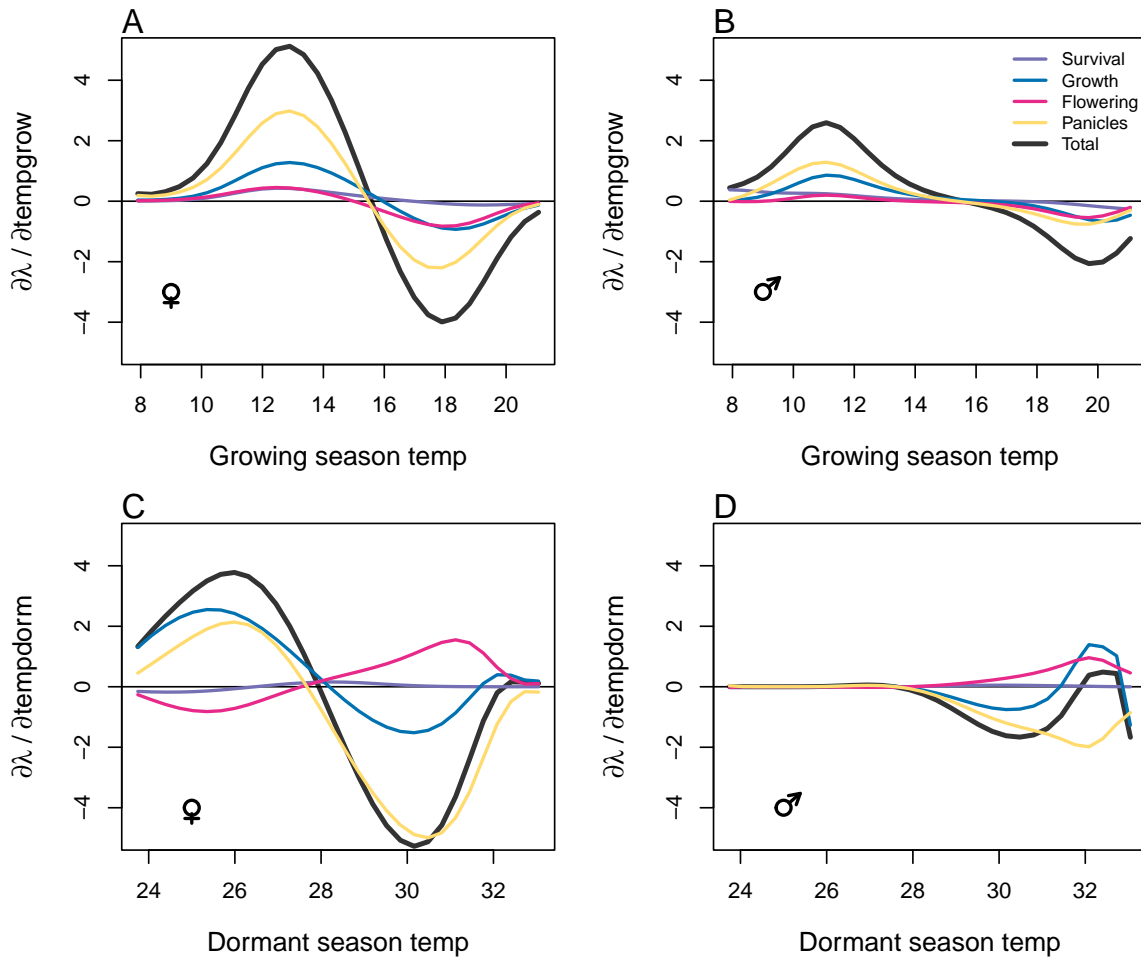


Fig. S10. Life table response experiment decomposition of the sensitivity of λ to seasonal climate into additive vital rate contributions of males and females based on posterior mean parameter estimates. (A) Temperature of growing season (contribution of female), (B) Temperature of growing season (contribution of male), (C) Temperature of dormant season (contribution of female) and (D) Temperature of dormant season (contribution of male).

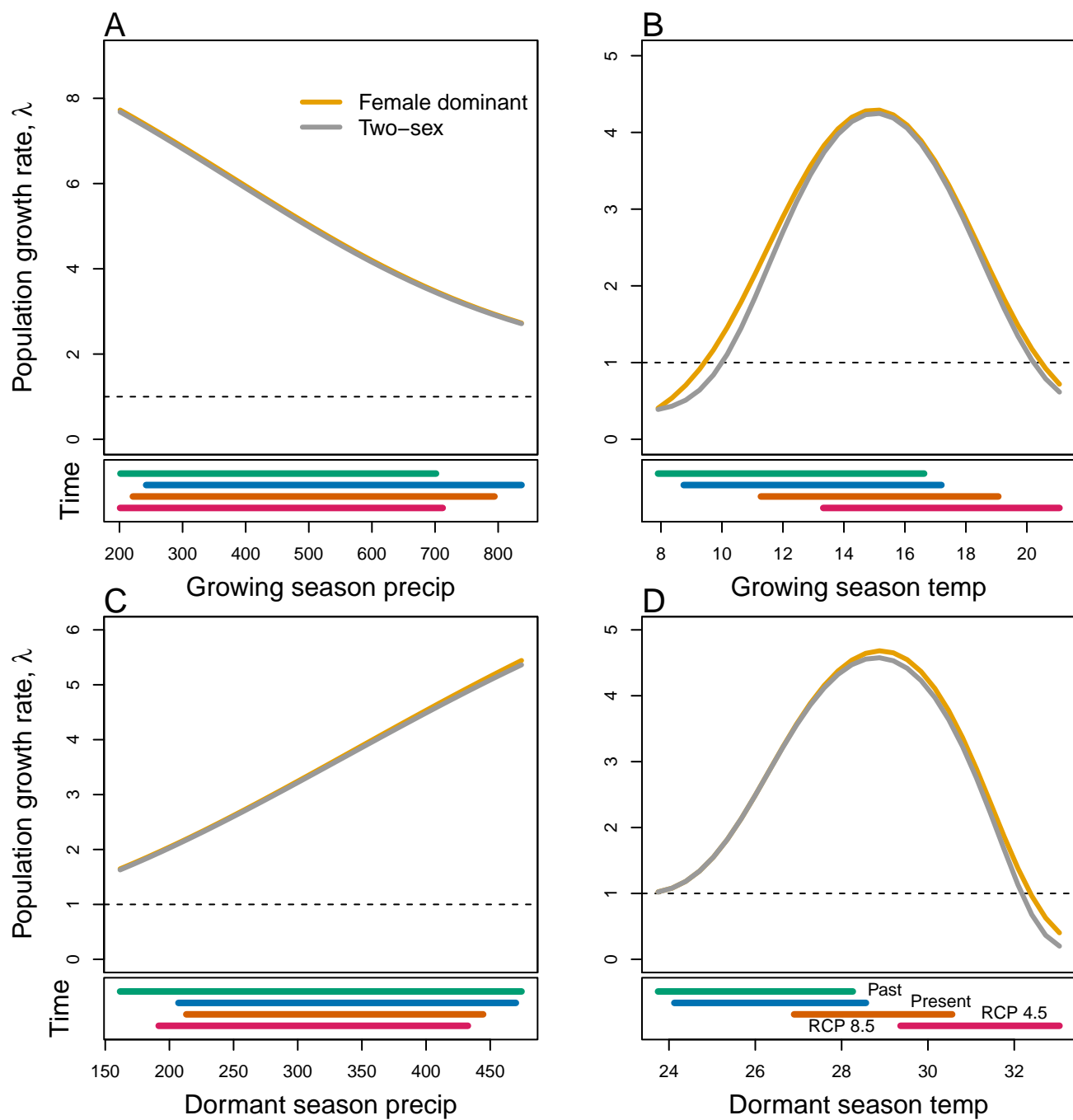


Fig. S11. Predicted population growth rate (λ) in different ranges of climate. (A) Precipitation of the growing season, (B) Temperature of the growing season, (C) Precipitation of the dormant season, (D) Temperature of the dormant season. The grey curve shows prediction by the two-sex matrix projection model that incorporates sex-specific demographic responses to climate with sex ratio dependent seed fertilization. The orange curve represents the prediction by the female dominant matrix projection model. The dashed horizontal line indicates the limit of population viability ($\lambda = 1$). Lower panels below each data panel show ranges of climate values for different time period (past climate, present and future climates). For future climate, we show a Representation Concentration Pathways (RCP) 4.5 and 8.5. Values population viability of (λ) are derived from the mean climate variables across 4 GCMs (MIROC5, ACCESS1-3, CESM1-BGC, CMCC-CM).

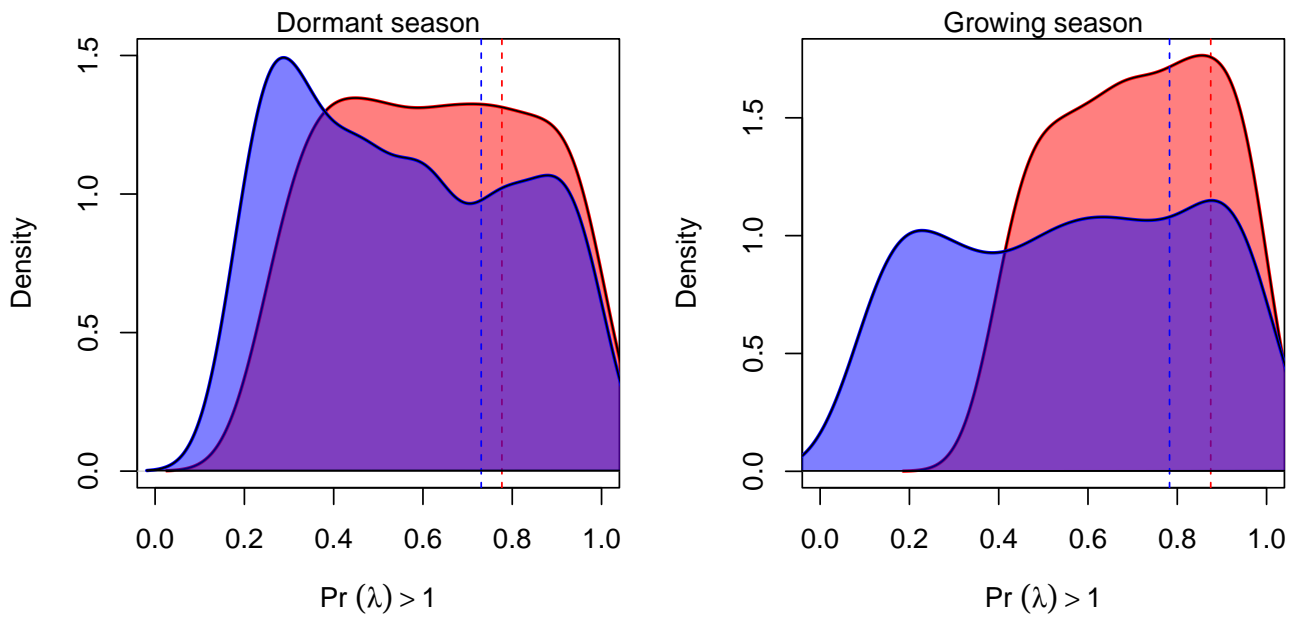


Fig. S12. Assessment of the statistical difference between the two-sex models and the female dominant model for the dormant and growing season. Plots show the density of $\text{Pr}(\lambda > 1)$ values for female dominant (pink) and two-sex models (violet) for each season. The means for each model are shown as vertical dashed lines.

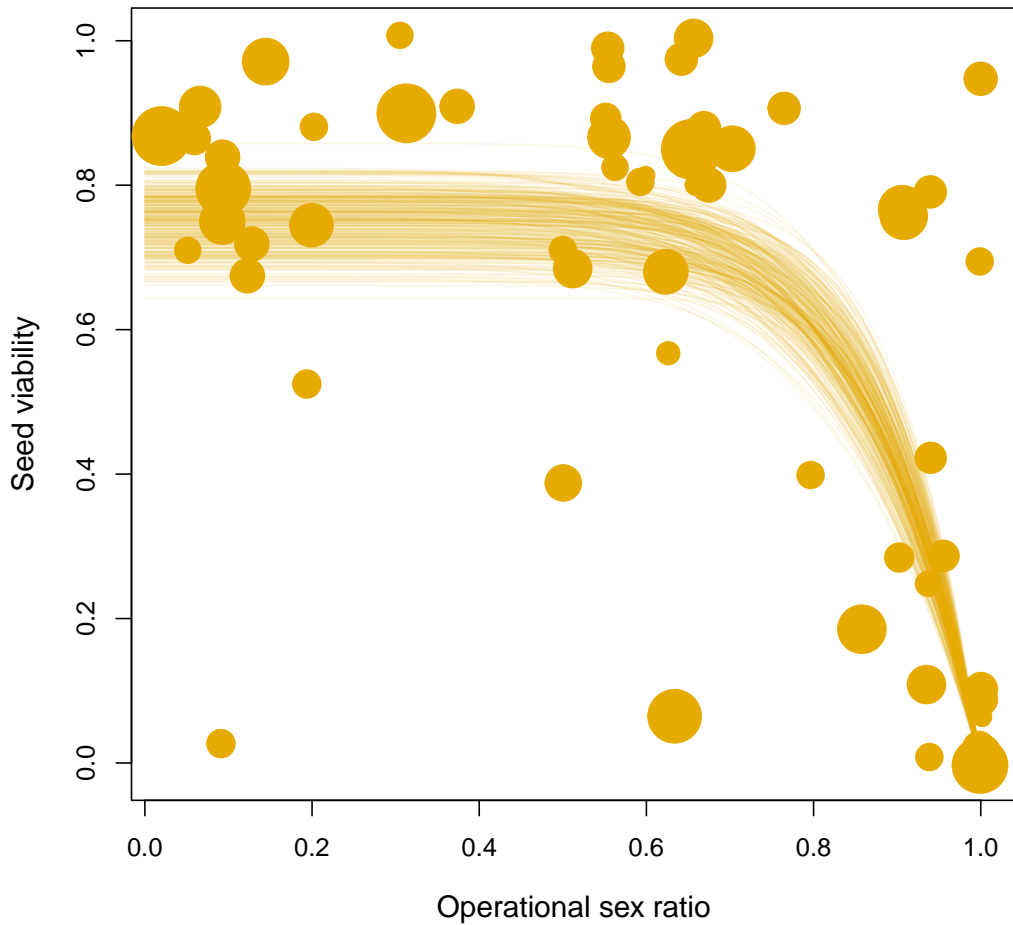


Fig. S13. Seed fertilization success as a function of operational sex ratio (fraction of panicles that are female) in experimental populations. Circles show data from tetrazolium assays of seed viability; circle size is proportional to the number of seeds tested (minimum: 14; maximum: 57). Lines show model predictions for 300 samples from the posterior distribution of parameter estimate

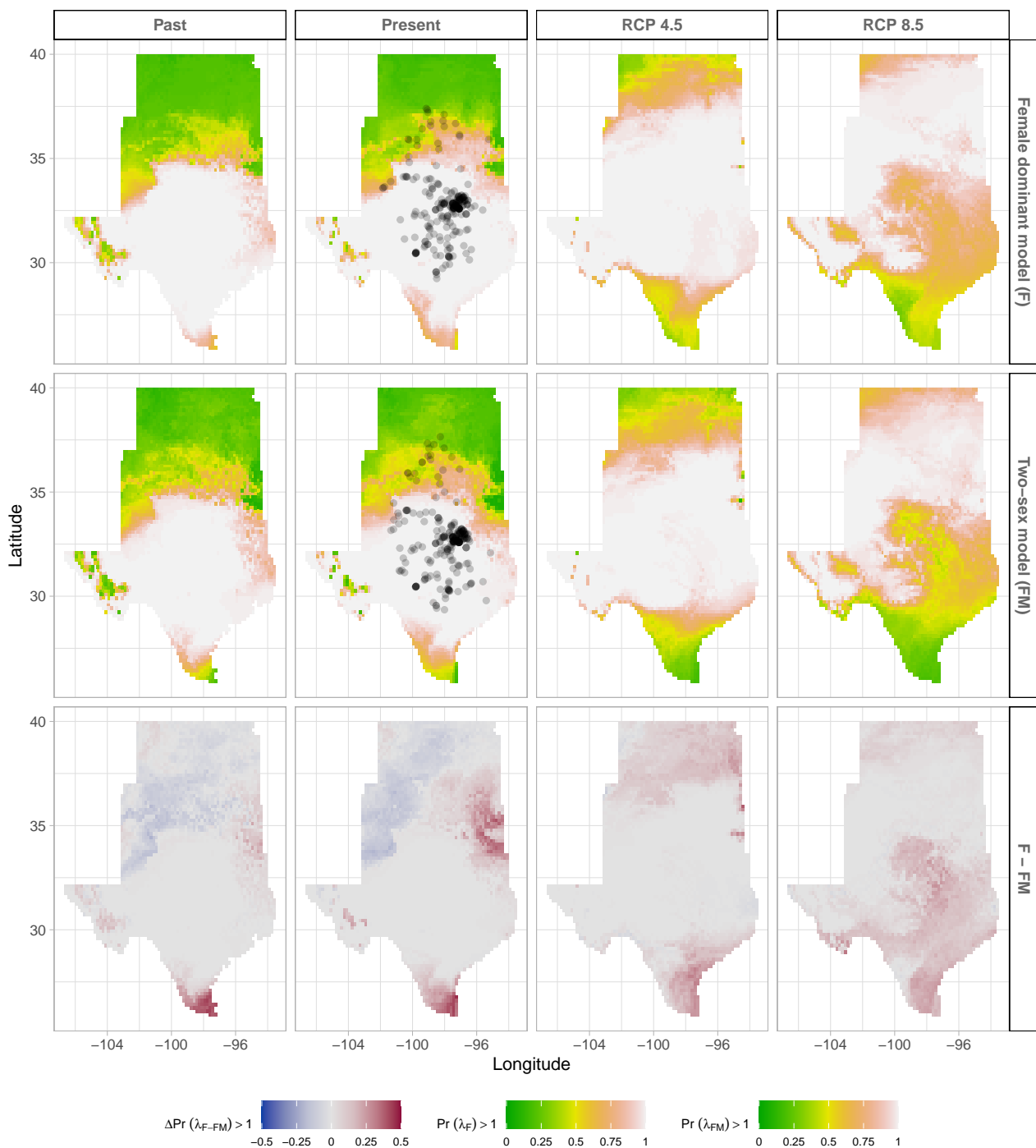


Fig. S14. Climate change favors range shift toward the North edge of the current range. (A) Past, (B) Current, (C and D) Future predicted range shift based on the predicted probabilities of self- sustaining populations, $\text{Pr}(\lambda > 1)$, using the two-sex model that incorporates sex- specific demographic responses to climate with sex ratio dependent seed fertilization. (E) Past, (F) Current, (G and H) Future predicted range shift based on the predicted probabilities of self- sustaining populations, $\text{Pr}(\lambda > 1)$, using the female dominant model. Future projections were based on the CESM1-BGC model. The black dots on panel B and F indicate all known presence points collected from GBIF from 1990 to 2019, which corresponds to the current condition in our prediction. The occurrences of GBIFs are distributed in with higher population fitness habitat $\text{Pr}(\lambda > 1)$, confirming that our study approach can reasonably predict range shifts.

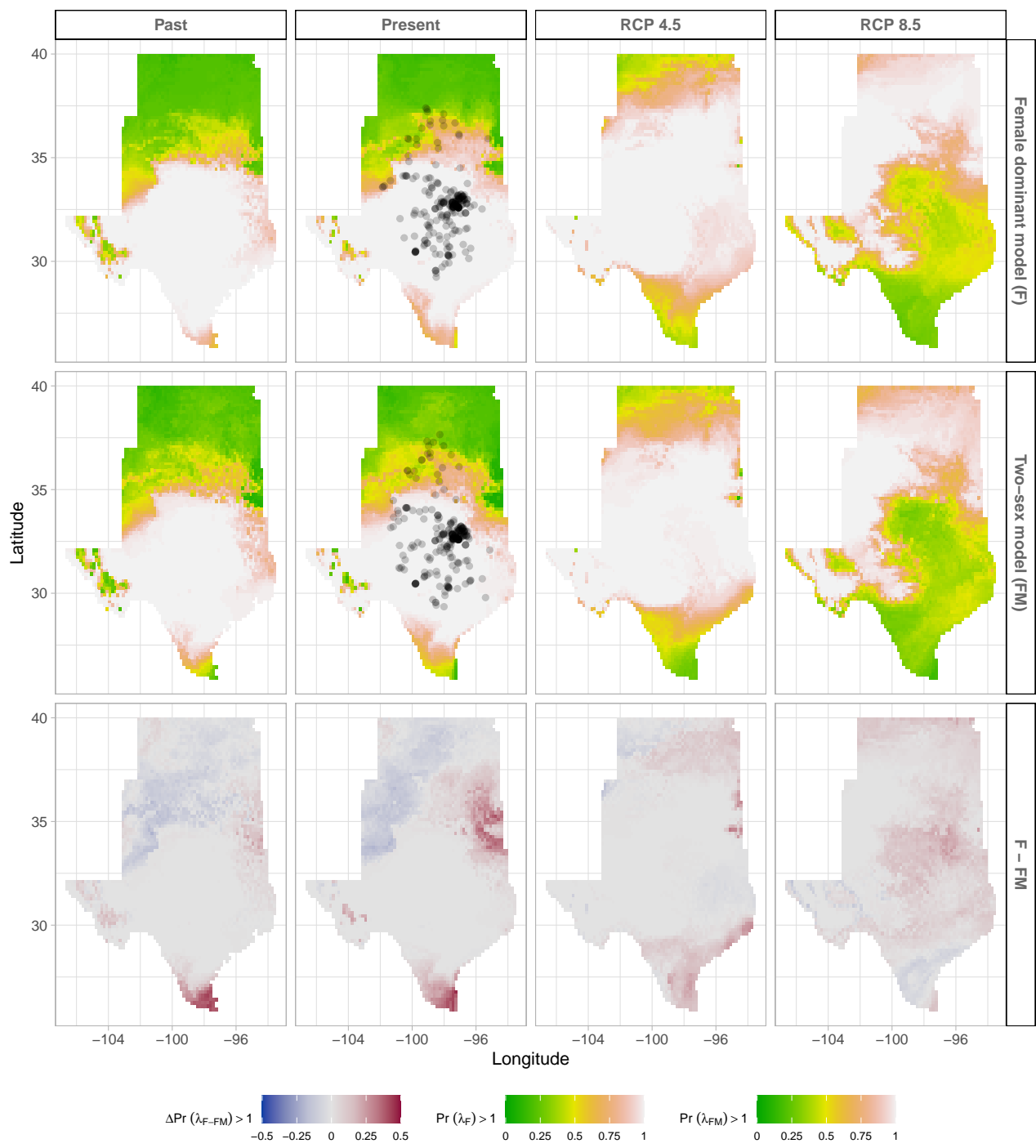


Fig. S15. Climate change favors range shift toward the North edge of the current range. (A) Past, (B) Current, (C and D) Future predicted range shift based on the predicted probabilities of self-sustaining populations, $\text{Pr}(\lambda > 1)$, using the two-sex model that incorporates sex-specific demographic responses to climate with sex ratio dependent seed fertilization. (E) Past, (F) Current, (G and H) Future predicted range shift based on the predicted probabilities of self-sustaining populations, $\text{Pr}(\lambda > 1)$, using the female dominant model. Future projections were based on the ACCESS model. The black dots on panel B and F indicate all known presence points collected from GBIF from 1990 to 2019, which corresponds to the current condition in our prediction. The occurrences of GBIFs are distributed in higher population fitness habitat $\text{Pr}(\lambda > 1)$, confirming that our study approach can reasonably predict range shifts.

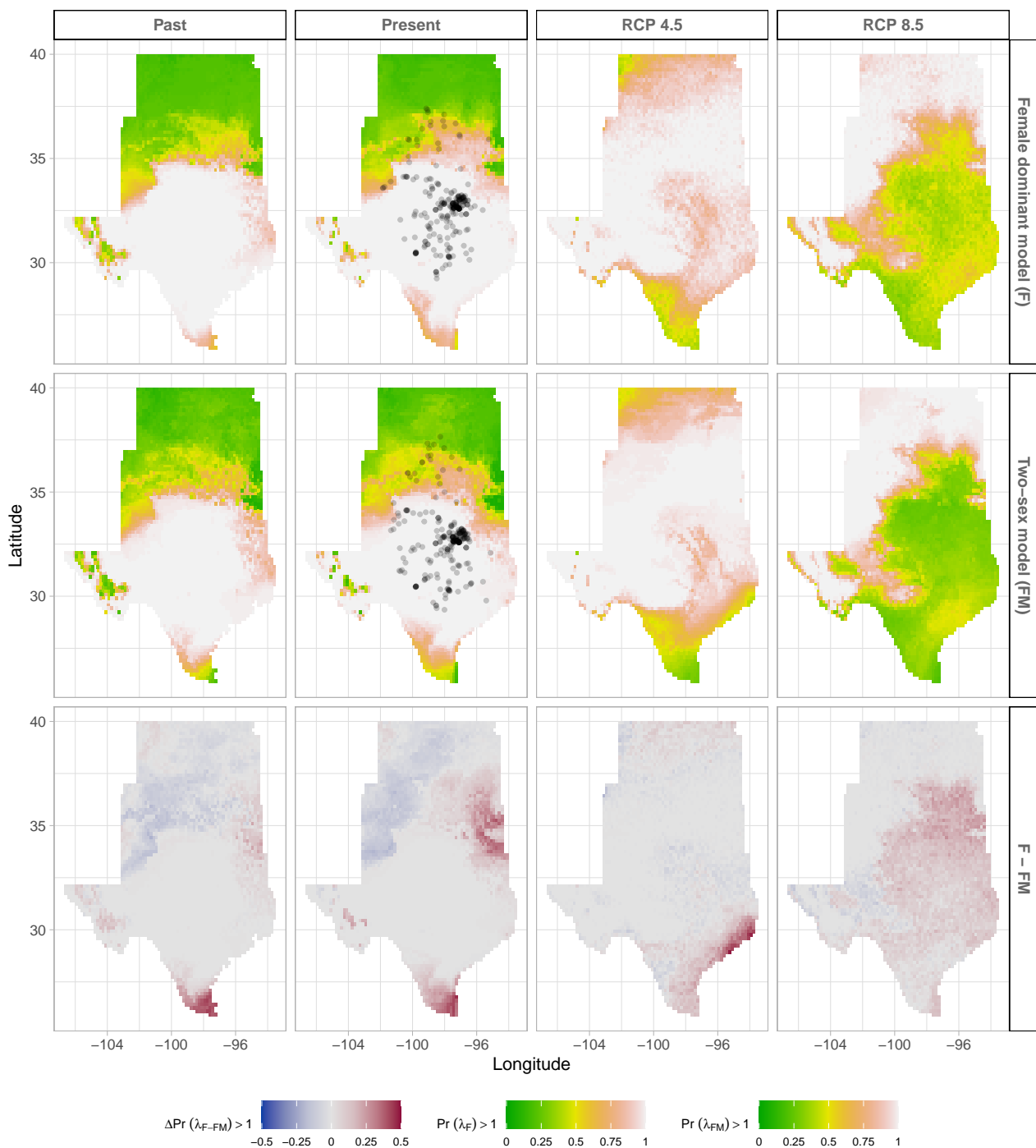


Fig. S16. Climate change favors range shift toward the North edge of the current range. (A) Past, (B) Current, (C and D) Future predicted range shift based on the predicted probabilities of self-sustaining populations, $\Pr(\lambda > 1)$, using the two-sex model that incorporates sex-specific demographic responses to climate with sex ratio dependent seed fertilization. (E) Past, (F) Current, (G and H) Future predicted range shift based on the predicted probabilities of self-sustaining populations, $\Pr(\lambda > 1)$, using the female dominant model. Future projections were based on the MIROC5 model. The black dots on panel B and F indicate all known presence points collected from GBIF from 1990 to 2019, which corresponds to the current condition in our prediction. The occurrences of GBIFs are distributed in with higher population fitness habitat $\Pr(\lambda > 1)$, confirming that our study approach can reasonably predict range shifts.

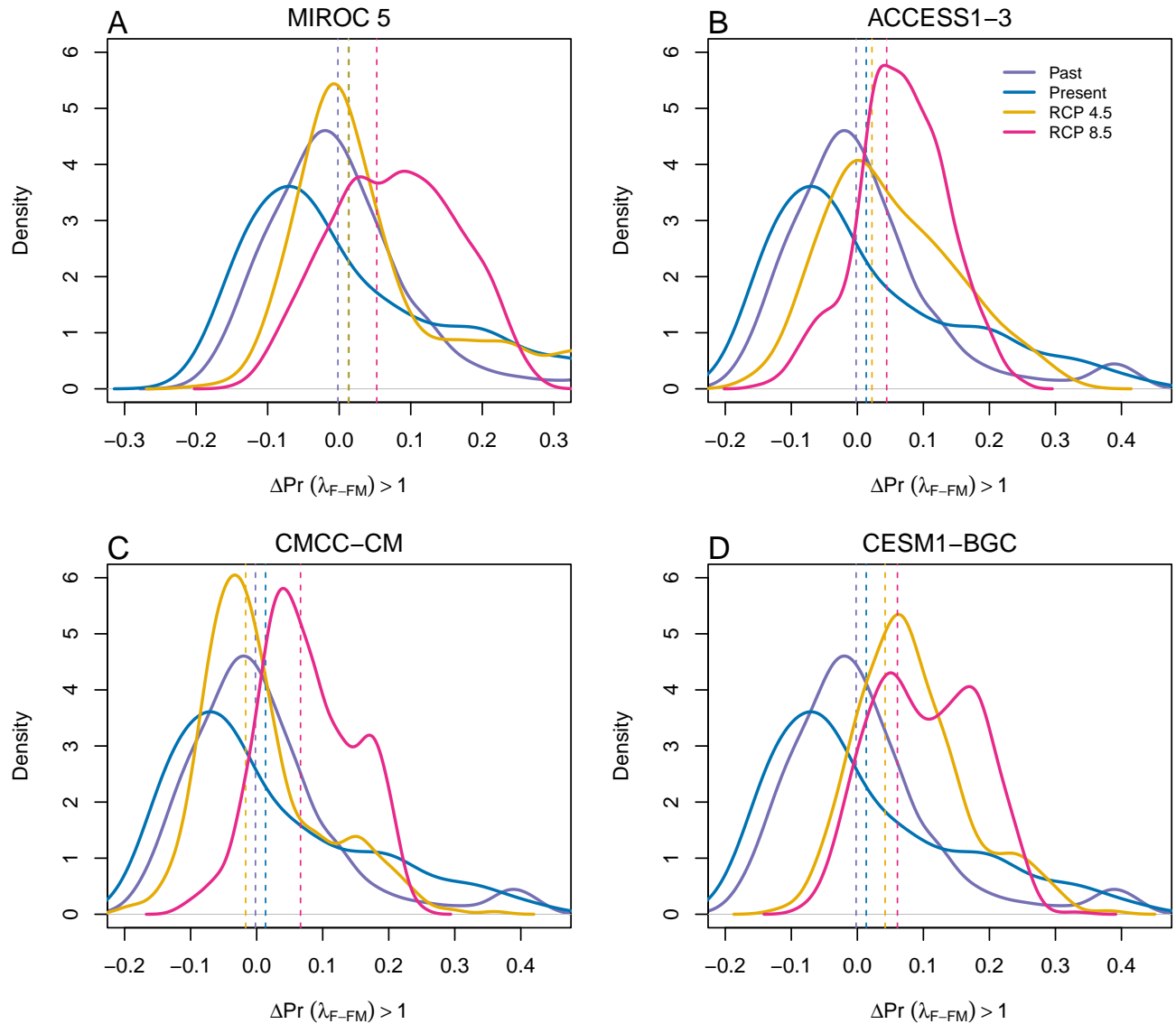


Fig. S17. Assessment of the statistical difference between the two-sex models and the female dominant model across and beyond species range for 4 GCMs. The means for each model are shown as vertical dashed lines.

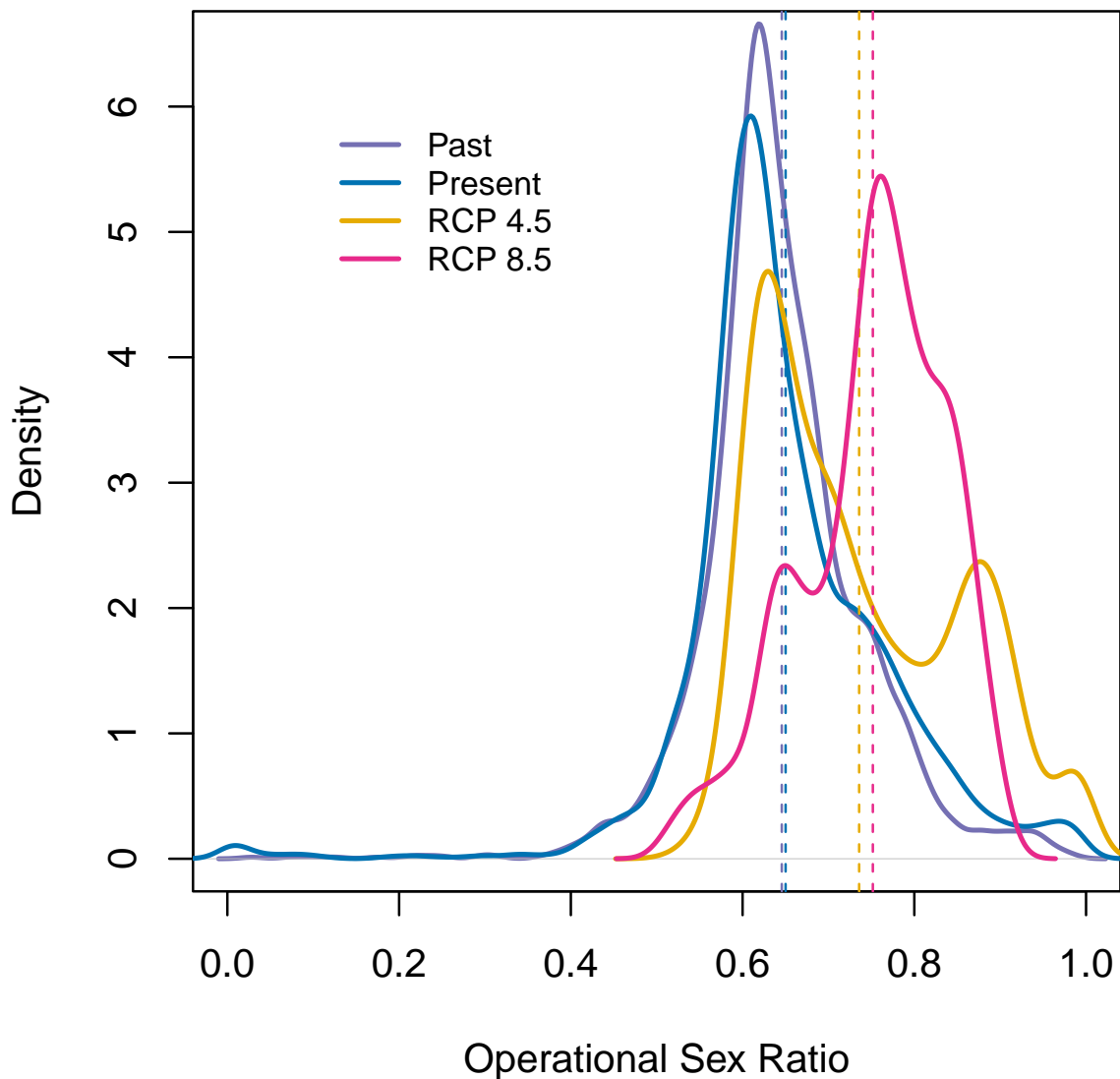


Fig. S18. Change in Operational Sex Ratio (proportion of female panicle) over time (past, present, future). Future projections were based on the CMCC-CM model. The mean sex ratio for each time period is shown as vertical dashed line.

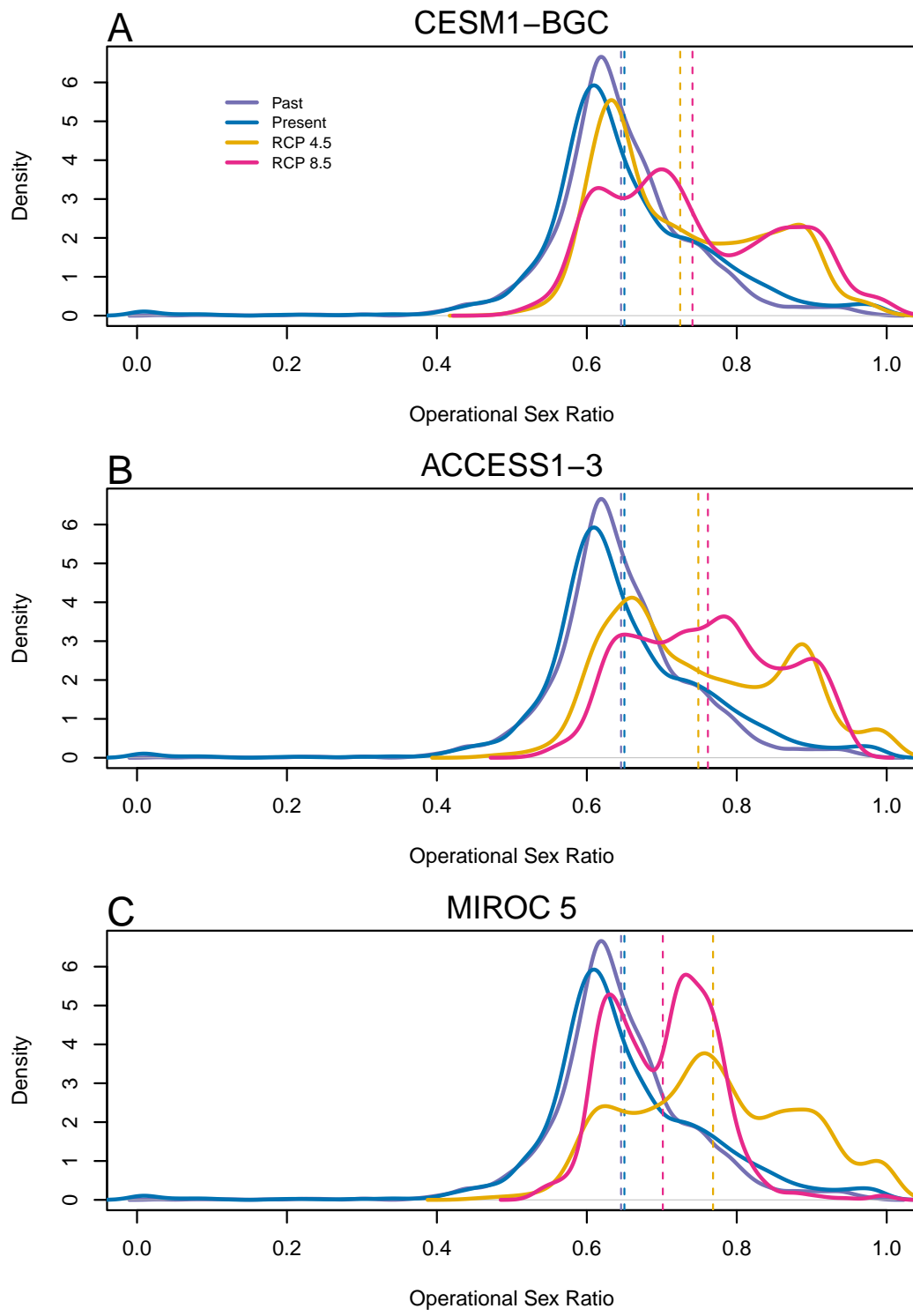


Fig. S19. Change in Operational Sex Ratio (proportion of female) over time (past, present, future). Future projections were based on A) MIROC 5, B) CES, C) ACC. The means for each model are shown as vertical dashed lines.

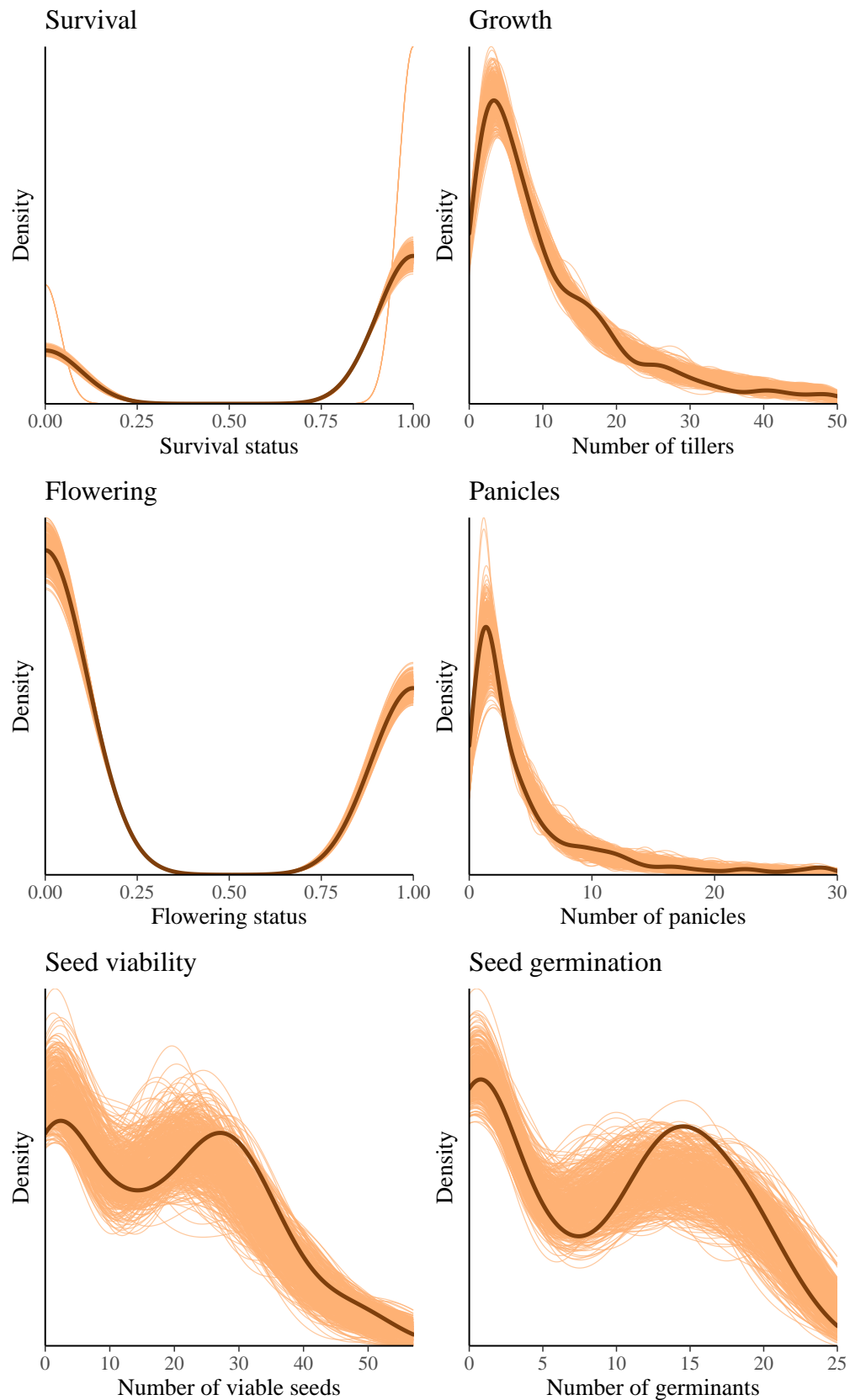


Fig. S20. Posterior predictive checks. Consistency between real data and simulated values suggests that the fitted vital rate models accurately describes the data. Graph shows density curves for the observed data (light orange) along with the simulated values (dark orange).

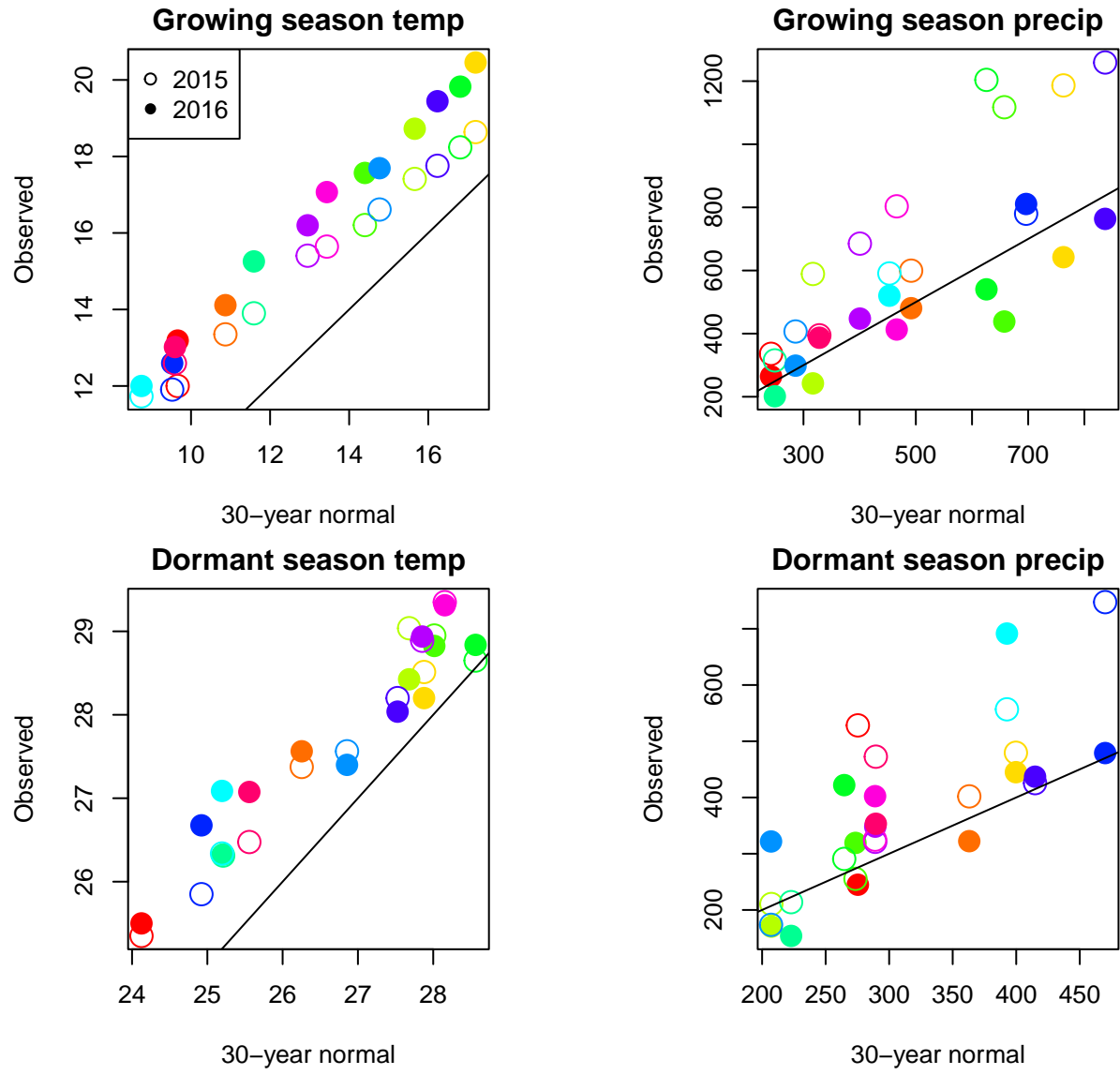


Fig. S21. Comparison of 30-year (1990–2019) climate normals and observed weather conditions at common garden sites during the 2014–15 and 2015–16 census periods. Temperature is in °C and precipitation is in mm. Colors represent sites and lines show the $y = x$ relationship.

67 **References**

- 68 1. Benjamin M Sanderson, Reto Knutti, and Peter Caldwell. A representative democracy to reduce interdependency in a
69 multimodel ensemble. *Journal of Climate*, 28(13):5171–5194, 2015.
- 70 2. Allison M Thomson, Katherine V Calvin, Steven J Smith, G Page Kyle, April Volke, Pralit Patel, Sabrina Delgado-Arias,
71 Ben Bond-Lamberty, Marshall A Wise, Leon E Clarke, et al. Rcp4. 5: a pathway for stabilization of radiative forcing by
72 2100. *Climatic change*, 109:77–94, 2011.
- 73 3. Christopher R Schwalm, Spencer Glendon, and Philip B Duffy. Rcp8. 5 tracks cumulative co2 emissions. *Proceedings of the
74 National Academy of Sciences*, 117(33):19656–19657, 2020.
- 75 4. Aldo Compagnoni, Kenneth Steigman, and Tom EX Miller. Can't live with them, can't live without them? balancing
76 mating and competition in two-sex populations. *Proceedings of the Royal Society B: Biological Sciences*, 284(1865):20171999,
77 2017.
- 78 5. Tom EX Miller and Aldo Compagnoni. Two-sex demography, sexual niche differentiation, and the geographic range limits
79 of texas bluegrass (poa arachnifera). *The American Naturalist*, 200(1):17–31, 2022.